Development of a Hydraulic Resistance Correlation for the Heat Exchangers in a Pool-type Sodium-cooled Fast Reactor

Churl Yoon*, Huee-Youl Ye, Jae Hyuk Eoh
Advanced Reactor Technology Development Division, Korea Atomic Energy Research Institute,
111 Daedeok-daero 989 Beon-gil, Yuseong-gu, Daejeon 34057, Korea
**E-mail: cyoon@kaeri.re.kr*

***Keywords :** sodium-cooled fast reactor (SFR) , SALUS, computational fluid dynamics (CFD), porous media approach, hydraulic resistance

1. Introduction

SALUS (Small, Advanced, Long-cycled and Ultimate Safe SFR) is a pool-type sodium-cooled fast reactor generating 100MWe with a long refueling period of around 20 years, which is currently being designed in Korea Atomic Energy Research Institute (KAERI).[1] The PHTS (Primary Heat Transfer System) of a SALUS reactor includes two coolant pumps, four IHXs (Intermediate Heat Exchangers), and four DHXs (Decay Heat Exchangers), which was developed from the PGSFR (Proto-type Generation-IV Sodium-cooled Fast Reactor) design as a reference.

Yoon, et al. [2] performed CFD (Computational Fluid Dynamics) analyses to get the fluid flow field and temperature distribution over the SALUS PHTS being directly contact with HAA (Head Access Area) and RVCS (Reactor Vault Cooling System), of which the results were used as input data to the structural analyses for developing and confirming the SALUS design. In the CFD modelling, the secondary loops of all the IHXs and DHXs were ommitted and the shell-side tube bundles flow regions were approximated as porous media having proper hydraulic resistances and heat removal rates. A commercial CFD software vended by Siemens Corp., STAR-CCM+ Version 16.02 [3], was used for the CFD analyses as like the current study.

Kong, et al. [4] investigated experimentally the flow characteristics at the shell side of a prototype intermediate heat exchanger (p-IHX) in a PGSFR. The pressure drop at the shell side of the p-IHX under a wide range of flow rate conditions was determined by using the pressure drop measurements from the iHELP (Intermediate Heat Exchanger test Loop for PGSFR) and the IEC (Intermediate heat exchanger test loop for Exit flow Channel) test facilities.

In the current study, a hydraulic resistance correlation for the shell-side fluid flows in the PGSFR IHXs and DHXs has been developed as a form of the combination of a conventional correlation for the axial flow along a straight tube bundle and the pressure drop correlation across a grid plate. The developed correlation was adjusted and verified by utilizing the pressure drop measurements in the iHELP experimental facility, so that the correlation could take account of the varying Reynolds number effect according to the reactor power level changes. Finally, the developed hydraulic rersistance correlation was verified by implementing the correlation into the CFD models and comparing the simulated pressure drop results with the iHELP experimental data. The developed hydraulic resistance correlation would be applied for the SALUS design optimization in the future studies.

Table 1: Thermal Design Parameters of the SALUS HXs

Parameter	IHX	DHX
Number of units	4	4
Rated heat removal capacity per unit	97.8 MW_t	1.67 MW_t
Number of tubes per unit	1050	114
Total tube length	4.85 m	2.13 m
Active tube length	3.8 m	1.73 m
Shroud inner diameter	1.311 m	0.576 m
Shell-side inlet temp.	510 ºC	360 ºC
Shell-side outlet temp.	357.7 ºC	251.1 ºC
Shell-side sodium flowrate	341.4 kg/s	11.74 kg/s
Heat transfer tube outer diameter	17.9 mm	21.7 mm
Pitch-to-diameter ratio	1.5	1.5
Heat transfer tube material	9Cr-1Mo-V	9Cr-1Mo-V
Number of tube support structure (axially)	5	2

2. Methodology and Experimental Data

The objects of this study are the SALUS heat exchangers. Thermal design parameters of the IHX and DHX have been produced complying with the design requirements for the fluid system of 100 MWe SALUS, as sumarized in Table 1. Cylindrical-shaped IHXs and DHXs are counter-current flow type sodium-to-sodium heat exchangers with a shell and straight tubes. Figure 1 shows a schematic design of the SALUS DHX, the design concept of which is similar to the SALUS IHX's. In the shell-and-tube type heat exchanger region, secondary sodium flows upward inside the heat transfer tubes and primary sodium flows downward parallel with the heat transfer tubes in the shell-side sodium flow path. After the heat transfers inside both the IHX and DHX

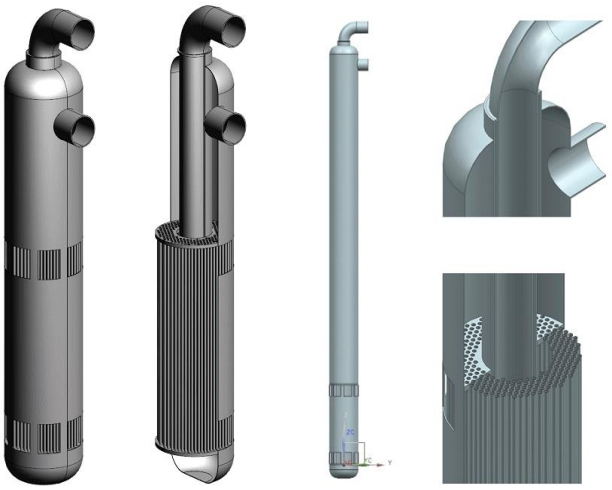

Fig. 1. Schematic design of the SALUS DHX.

tube bundle regions, primary sodium is discharged into the lower part of the cold sodium pool.

2.1 Porous Media Approaches for the Shell-side Flows of Heat Exchangers

In most CFD analyses of heat exchangers, the shell-side fluid flow regions are simplified as porous media having proper hydraulic resistances and heat removal rates instead of simulating all the detailed flows around every heating tube. The assumptions in the porous media approaches are that the control volumes and the control surfaces are large relative to the interstitial spacing of the porous medium, and that the given control cells and control surfaces are assumed to contain both the fluid and the distributed solids.

By defining the volume porosity as $\gamma \equiv \frac{\mathrm{Vol_f}}{\mathrm{Vol_T}}$ and the area porosity as $\gamma_A \equiv \frac{A_f}{A_T}$, Todreas and Kazimi [5] directly applied the conservation principles to derive the continuity, momentum, and energy equations for a porous medium.

When the cross-sectional views of a porous medium are uniform in an axial direction as like a tube bank, it could be assumed that $\gamma = \gamma_A$. Then, $\gamma \cdot u$ in the governing equations could be substituted with u^S, where the superficial velocity $u^S(=\gamma \cdot u)$ is an artificial flow velocity that assumes that only fluid passes the cross-sectional area neglecting the solid portion of the porous medium.[3]

The hydaulic resistance in the porous medium, that will be treated as a momentum source term, consists of the viscous (linear) and the inertial (quadratic) resistance terms.

$$R_i = -\frac{\Delta P}{\Delta L}\Big)_i = \frac{\mu}{K} u_i^S + K_{loss} \frac{\rho}{2} u_i^S \left| U^S \right| \qquad (1)$$

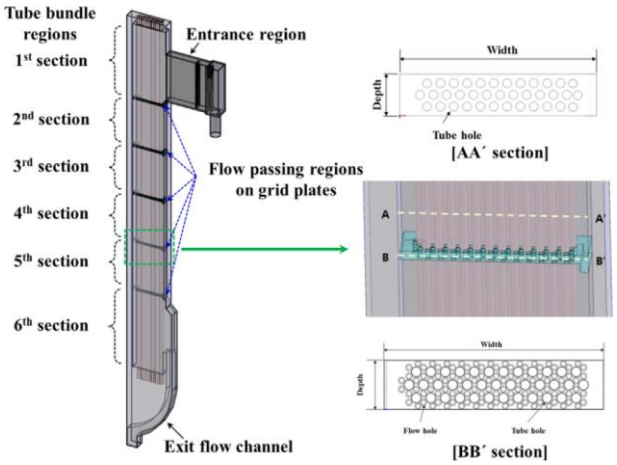

Fig. 2. Experiments test section in the iHELP test facility.

Here, μ, K, and K_{loss} are respectively dynamic viscosity, permeability, and pressure loss coefficient.

2.2 iHELP Experiment

The flow characteristics at the shell side of a p-IHX in a PGSFR were investigated experimentally by Kong et al.[4] The shell side of a p-IHX consisted of an inlet window, tube bundles, grid(support) plates, and an exit flow channel. Flow characteristics across the IHX, especially at the shell side, should be investigated and identified to design the IHX appropriately and to analyze accurately the performance and safety of a PGSFR. Primary sodium flows along the heat transfer tubes (HTTs) and across the five grid plates with flow holes for supporting the HTTs in the primary sodium flow path. For investigating the pressure drop at the tube bundle regions with the grid plates, a test facility named iHELP was constructed based on a 1/29.6 volumetric scale ratio. The experimental pressure drop results were obtained over a wide range of flow rate conditions, among which the nominal conditions have the same Reynolds number with the p-IHX. The experiments were conducted using water (35 °C, 0.1 MPa) instead of sodium (467.5 °C, 0.1 MPa) in the scaled-down test section. Since the geometric and dynamic similarities were preserved in the test loop and test section designs, Eq. (2) could be derived by the Euler number conservation with a constant Reynolds number referring to the p-IHX to convert the pressure drop at the iHELP into the pressure drop at the p-IHX.[4]

$$\Delta P_{p-IHX} = \Delta P_{iHELP} \left(\frac{\rho_{water}}{\rho_{sodium}} \right) \left(\frac{\mu_{sodium}^2}{\mu_{water}^2} \right) \qquad (2)$$

Fig. 2 shows the experimental test section of the iHELP test facility. Since the SALUS IHXs have different shapes of the IHX outlet windows from the PGSFR's, the measured pressure-drop values across only the 2nd, 3rd, and 4th sections out of five grid plats

were utilized for the verification procedure. The pressure probing distances ΔL's are uniformly 0.64m for these three pressure-drop measurements.

3. Hydraulic Resistance Model for Porous Media

In this section, the procedure of developing a hydraulic resistance correlation for the assumed porous media in the shell-side flow regions of IHXs and DHXs is described. At the end of this section, verification of the developed correlation against the iHELP experimental data is also presented.

3.1 Basic Hydaulic Resistance Correlations for the Shell-side Flows of the Heat Exchangers

In a CFD simulation for the SALUS heat exchangers, the pressure drops due to the frictional and form losses around structures such as the inlet/outlet windows, inner pipe, shroud, and etc. are accounted for by making the geometry of the computational domain in detail and adopting the grid-independent meshes on that geometry and proper analytic models. And, the pressure losses as the fluid goes through the shell-side region of the IHX or DHX are thought to be composed of three components: lateral(cross) flows pressure drop over the tube bundle, axial flows pressure drop along the tube bundle and pressure drop across the grid plates. In this study, it was assumed that the travelling lengths of the lateral flows were relatively short compared to the axial flows and their effects were neglegible. Thus, we can now say that the shell-side pressure loss of the heat exchangers inside the PHTS consists mainly of the frictional pressure losses along the straight tube bundle and the pressure drops across the grid(support) plates.

As the first one of the basic hydraulic resistance correlations, the pressure losses along a straight tube bundles of constant cross section can be expressed as a conventional internal pipe flow correlation with the simple Darcy friction factor correlation [6].

$$f_z = \begin{cases} \dfrac{64}{\mathrm{Re}} & \text{for } \mathrm{Re} < 2{,}000 \\ \dfrac{1}{\left[1.8\log\left(\mathrm{Re}\right) - 1.64\right]^2} & \text{for } \mathrm{Re} > 4{,}000 \end{cases} \quad (3)$$

where the Reynolds number is calculated by the internal pipe flow correlation of $Re = \rho uD/\mu$. Note that u here is the physical velocity, not superficial velocity. Between laminar (Re < 2,000) and turbulent (Re > 4,000) regimes, the friction factor for transition regime (2,000 ≤ Re ≤ 4,000) follows the graph (b) of Diagram 2-1 in Idelchik's handbook [6] and the values are listed in Table 2. The simplest polynomial fitting curve was derived for the friction coefficient of transition regime by utilizing OriginPro [7] software, as follows:

Table 2: Darcy Friction Coefficient for Transition Regime

Reynolds Number, *Re*	Friction Coefficient, f_z
2,000	0.032
2,500	0.034
3,000	0.040
4,000	0.040

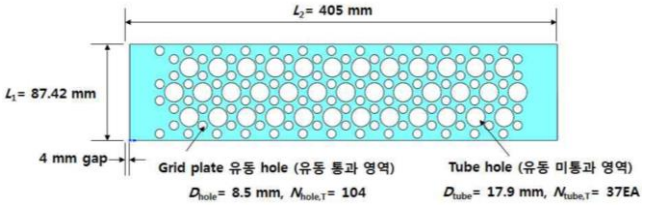

Fig. 3. Cross-sectional view of the iHELP grid(support) plate.

$$f_z = A + B_1\,\mathrm{Re} + B_2\,\mathrm{Re}^2 + B_3\,\mathrm{Re}^3 \quad for\ 2{,}000 \le \mathrm{Re} \le 4{,}000 \quad (4)$$

Here, A = 0.184, B_1 = -1.8E-4, B_2 = 6.8E-8, and B_3 = -8.0E-12.

For the shell-side flow channel with triangular tube array, the hydraulic diameter required for calculating Reynolds number is defined as Eq. (5) by considering axial flow channel area, A_f.

$$A_f = \frac{\sqrt{3}}{4}P^2 - \frac{1}{2}\times\frac{\pi}{4}d_{o,w}^2$$

$$D_h = \frac{4A_f}{\pi d_{o,w}/2} \quad (5)$$

where A_f, P, $d_{o,w}$ and D_h denote flow channel area, pitch between tube centers, tube outer diameter, and shell-side hydraulic diameter, respectively. Then, the axial frictional pressure drop is obtained by the following equation.

$$\Delta P_{axial} = f_z \frac{L}{D_h}\cdot\frac{1}{2}\rho u_{axial}^2 \quad (6)$$

The second basic hydraulic resistance correlation for the shell-side flows through PGSFR IHX or DHX is the pressure drop across the grid plates, which are installed with the same interval distance. As an example, the top view of the iHELP grid plate is presented in Fig. 3, in which 104 flow holes with a diameter of 8.5 mm are installed in equal spacing between the heating tube penetrations. These grid plates and their flow effects were also included in the porous regions in the CFD simulation. The estimated porosity of the porous support plate is 0.2292, as same as PGSFR. The pressure drop at the grid plate is modelled by the Diagram 3-12 in Idelchik[6] and Han[8], as follows:

$$\Delta P_{Grid} = K_i \frac{1}{2}\rho u^2 + \xi_{fr} \quad (7)$$

where $K_i = \frac{\Delta P}{\rho u_0^2 / 2} = \left(1.707 - \bar{f}\right)^2 \cdot \frac{1}{\bar{f}^2}$ (8)

Here, ξ_{fr} is the potential friction loss passing through the grid plate, u_o is flow velocity upstream, and $\bar{f}$ is the (actual flow area) to (frontal flow area) ratio.

In Eq. (7), the potential friction loss term ξ_{fr} could be ignored since the grid plate are very thin (The plate thickness is 20mm for IHX or 15mm for DHX.) compared to overall length scales. Here, it should be noted that the constant K_i in Eq. (7) & (8) is expressed as a function only of geometric data, not a function of a flow condition such as Reynolds number. On the other hand, the constant f_z in Eq. (6) is a function of Reynolds number.

3.2 Development of the Hydaulic Resistance Correlation

In this study, the total hydraulic resistance of the shell-side flows in the SALUS IHX or DHX were expressed as a combination of the axial frictional pressure losses along the heating tubes (Eq. (6)) and the pressure drops cross the grid plates (Eq. (7)). The correction of the combined correlation is performed by utilizing the iHELP experimental data.

The total axial pressure drops of the shell-side flows in the SALUS heat exchangers are expressed as follows:

$$\Delta P_{total} = \Delta P_{axial} + F \cdot \Delta P_{Grid} \quad (9)$$

where F is a correction factor. This correction factor modifies the simple conventional pressure drop correlation of Eq. (7) into a realistic correlation reflecting the effect of Reynolds number. While the Idelchik's pressure drop correlation across a grid plate is one for a circular pipe flow containing a perforated plate, the grid(support) plates installed in the SALUS IHX and DHX contain the gap and heating tube penetrations as well as flow holes. To obtain the correction factor F, the iHELP experimental data were used as the reference values.

Figure 3 shows the cross-sectional view of the iHELP support plate and the dimensions, which is the same as the right bottom figure of Fig. 2. Note that there exists a 4mm-wide gap near the central downcomer pipe. Important parameters to calculate the pressure drops are summarized as in Table 3. For examples, the axial flow area (A) is calculated as follows:

$$A = 405mm \times 87.42mm - 37 \times \pi \left(\frac{17.9mm}{2}\right)^2$$
$$= 0.02609m^2$$

And, the periphrial length (Per) is also calculated as

$$Per = 2 \times (405mm + 87.42mm) + 37 \times \pi \times 17.9mm$$
$$= 3.06552m$$

Table 3: Calculated Parameters for iHELP Experiment

Parameter	Value
Channel (Porous) Region	
Porosity (volume)	0.73702
Number of heating tubes	37
Axial flow area (A)	0.02609 m^2
Peripherial length (Per)	3.06552 m
Hydraulic diameter (D_h = 4A/Per)	0.03405 m
Support (Grid) Plate	
Number of flow holes	104
Gap area	0.00035 m^2
Total area (except gap area)	① 0.03506 m^2
Total tube penetration area	② 0.00931 m^2
Total flow hole area	③ 0.00590 m^2
$\bar{f}$ in Eq. (8) = ③/(①-②)	0.2292
K_i in Eq. (8)	~ 41.53

With the calculated parameters in Table 3, the axial frictional pressure losses and the pressure drops across a grid plate per unit length (= 0.64m) were estimated for every flow condition of various power level from 1 ~ 113 %. Then, by equating the total pressure drops of Eq. (9) with the iHELP measured pressure drops, the target F values are derived as Table 4. In this calculation, water is the working fluid as like the iHELP experiment, of which viscosity and density are respectively 7.208E-4 Pa·s and 994.0 kg/m^3 at the average temperature of 35.0 ^oC. Finally, a simple fitting curve was obtained as a form of the exponential functions of Reynolds number by using OriginPro [7] software, as follows:

$$F = Y_0 + A_1 \exp(-\mathrm{Re}/T_1) + A_2 \exp(-\mathrm{Re}/T_2) \quad (10)$$

Here, Y_0 = 0.28461, A_1 = 0.12876, A_2 = 4971.3016, T_1 = 8895.01778 and T_2 = 80.68048.

3.3 Verification of the Developed Hydaulic Resistance Correlation

For the verification of the developed hydraulic resistance correlation, the CFD simulations for the iHELP experiment were performed. To simulate only the vertical section of the iHELP test section, a rectangular channel geometry was generated as shown in Fig. 4(a). The channel was a duct with a rectangluar cross section of 0.405 × 0.08742 m^2 and a total length of 3.308 m, which contains a porous region with a length of 2.774 m. In the figure, "g" denotes the gravitational force and the red arrows represent the inlet and outlet flows. The meshes of totally ~20,000 cells were generated all over the inlet, porous, and outlet regions. The k-ε turbulence model with two-layer all y+ wall treatment was adopted for the case that the channel flows passing through a porous region became turbulent. The vertical heating tube bundle was modeled as the

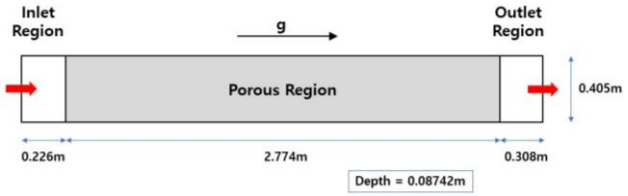

(a) Channel geometry for the CFD simulation

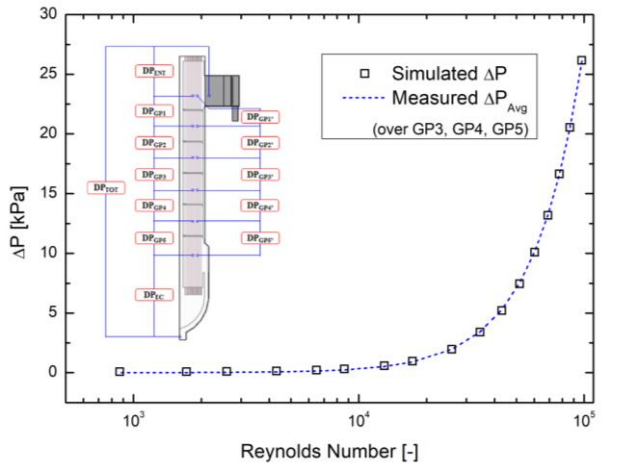

(b) Simulated pressure losses over ΔL (0.63m) compared with the iHELP experiments

Fig. 4. Verification of the modification factor by using CFD simulations.

porous region with a volume porosity of 0.73702, in which the developed hydraulic resistance correlation was implemented.

For the implemention of the developed hydraulic resistance correlation, the pressure loss rates were converted into the momentum source terms by dividing Eq. (9) by the travelling length. At this time, note that the STAR-CCM+ users should be careful as entering the input values for the "Porous Inertial Resistance", since the required input value is a coefficient(multiplier) to a square of the superficial velocity (= $\beta^2 u^2$) at each location and in the unit of kg/m^4.[2] Thus, the final form of the "Porous Inertial Resistance" becomes as follows:

$$\Delta P/\Delta L = \boxed{f_z \frac{1}{2D_h}\cdot\frac{\rho}{\beta^2} + K_i \frac{1}{2\Delta L}\cdot\frac{\rho}{\beta^2}\times F} * \beta^2 u^2 \quad (11)$$

Here, β is the porosity and ΔL is the distance where the pressure differences were measured. The values in the black-lined box are the user input to the "Porous Inertial Resistance" in STAR-CCM+ software. It should be noted that each term in the box was divided by β^2 to make Eq. (11) become the desired formulation.

From the simulation results of varyious mass flow rate according to the power level, the pressure drop rates along the central vertical line were extracted and compared with the average pressure drop of the differential pressure measurements over the GP (grid plate) 2~4, as presented in Fig. 4(b). Table 5 summarizes the verification simulation results, compared with the experimental measurements. The resultant y+ value range are very wide from below 10 to a few hundreds, which are acceptable by the applied wall treatment of 'two-layer all y+ wall treatment.' The 'two-layer all y+ wall treatment' is said to be suitable for the wall-cell contriods in the buffer region (1 < y+ < 30) as well as the log layer (y+ > 30) and the viscous sublayer (y+ < 1).[3] The differences between the measured and simulated pressure drops over the equal travelling length of 0.64m were proven to be less than 1.5% for the power level range of 30 ~ 113%. Since the target and final power level of this research is above 30% of the full power, the simulation results are satisfactory. Therefore, it is concluded that the developed hydraulic resistance correlation would work properly in the CFD simulations. It is thought that the large errors in the low power and mass flow conditions were caused by the inaccuracy of the lower-order fitting function (Eq. (10)) for the correction factor *F*. This lower-order fitting function was chosen for computational efficiency. In the application procedure, a higher-order fitting function would be tried if needed.

4. Application of the Developed Correlation to the CFD analyses for SALUS design

In this study, a realistic hydraulic resistance correlation for the porous media approaches in the SALUS CFD analyses has been developed by utilizing the pressure drop measurement performed in the iHELP experimental facility. In the previous CFD analyses of Yoon, et al. [2], the mass flow rates and heat removal rates of the SALUS heat exchangers were determined by 1-D system code or design code such as MARS-LMR and SHXSA [8], and set as constant values through the iterative computation precedure. However, in real situations the shell-side mass flow rates of the SALUS IHX or DHX are determined by the heat removal rate of

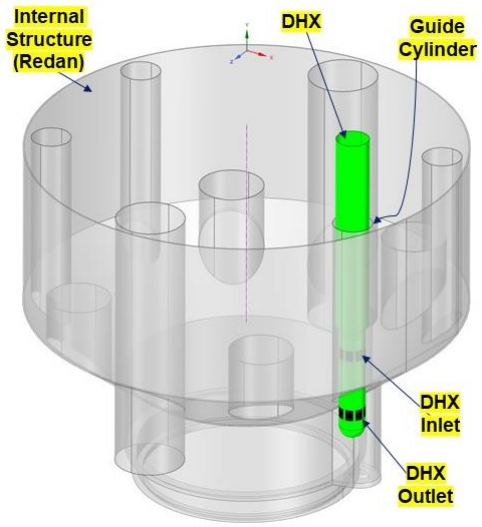

Fig. 5. Current SALUS layout of a DHX and the internal structure (Redan).

the secondary side (the induced bouyancy forces) and the shell-side flow chracteristics (the hydraulic resistance). Applying the proper hydraulic resistance and heat removal rate instead of adopting the mass flow rate and heat removal rate would make the CFD simulation more realistic and capable of accounting for the shell-side flow rate changes due to the surrounding thermal-fluidic conditions.

Figure 5 shows the current SALUS layout of a DHX and the internal structure (redan). Each DHX is placed inside a narrow guide cylinder, so that it is concerned if the hotter sodium could be continuously supplied to the DHX inlets or if the shell-side flows are not interrupted. Thus, one of the key issues in designing the SALUS becomes the effect of such a compact structural configuration around the DHX primary side inlets. Therefore, optimization study of the DHX elevation could be the object of the next research step, and the following procedures would be conducted:

1) The developed hydraulic resistance correlation will be converted for the SALUS application by applying the fluid properties of sodium and reflecting the design changes from PGSFR to SALUS. Then, the correlation will be implemented into the CFD model for the SALUS PHTS, based on the technical experiences in this study.
2) Ignoring any asymmetric effect to the DHX shell-side flows, a 1/4 CFD model of the SALUS PHTS will be generated for efficient and economical sensitivity study of the elevation of the SALUS DHX installation. Figure 6 presents a steady-state calculation result of the 1/4 PHTS model.
3) With the 1/4 PHTS model, CFD simulations will be performed for the cases of various DHX elevations, which is a part of the SALUS design optimization.
4) Finally, effects of the DHX elevation on their cooling capability in the SALUS cold pool will be analyzed under accident conditions as well as the full power operating condition.

5. Conclusions

In this study, a hydraulic resistance correlation of the porous media approaches for SALUS CFD analyses has been developed by utilizing the iHELP experimental data and verified by simulating the pressure drops over the vertical channel geometry of the iHELP test section. The developed hydraulic resistance correlation and the knowledge obtained in this study will be applied to the future researches such as the SALUS design optimization of DHX installation elevation and etc.

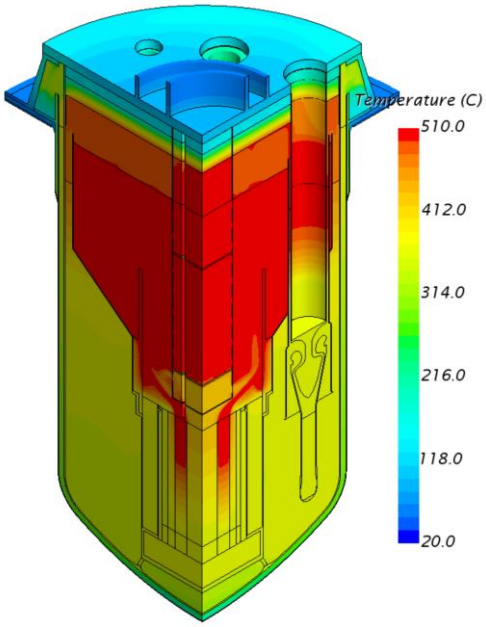

Fig. 6. Steady-state temperature distribution for the 1/4 SALUS PHTS model under a full power operating condition.

ACKNOWLEDGMENTS

This work was supported by the National Research Foundation of Korea (NRF) grant funded by the Korea government (MSIT). (No. 2021M2E2A1037871)

REFERENCES

[1] J. Eoh, C.-G. Park, J.-Y. Lim, J.-H. Kim, H.-Y. Ye, and J. Chang, “Design and Safety Features of SALUS-100: A Long Fuel-cycled Sodium-cooled Fast Reactor,” *Nuclear Engineering and Design*, Vol. 420, 112996, 2024.
[2] Churl Yoon, Huee-Youl Ye, and Jae Hyuk Eoh, “Hydraulic Resistance Modelling of the Porous Media Approaches for a Pool-type Sodium-cooled Fast Reactor,” KNS Spring Meeting, Jeju, 2024.
[3] Siemens Corp., STAR-CCM+ Version 16.02.008: Theory Manual, 2021.
[4] M. Kong, W. S. Kim, H. J. Chung, H.S. Choi, J. Kim, T. H. Lee, and D.-J. Euh, “Experimental Identification of Pressure Drop Characteristics at the Shell Side of an Intermediate Heat Exchanger inside a Prototype Generation-IV Sodium-cooled Fast Reactor,” *Nuclear Engineering and Design*, Vol. 348, pp. 177-186, 2019.
[5] N.E. Todreas and M.S. Kazimi, *Nuclear System II: Elements of Thermal Hydraulic Design*, Chap. 5, Hemisphere Publishing Corporation, 1990.
[6] I.E. Idelchik, *Handbook of Hydraulic Resistance*, ACE-TR-6630, 1960.
[7] OriginLab Corporation, OriginPro Ver. 8.0, http://www.OriginLab.com.
[8] J.G. Han, “SHXSA 1.2 SVVR,” KAERI Design Document, SAL-200-E2-472-001, 2021.

Table 4: Derivation of the Correction Factor *F* in Equation (9)

Power Level [%]	Mass Flow Rate [kg/s]	Calculation				Measured (iHELP) $(\Delta P/\Delta L)_{Total}$ [Pa/m]	Correction Factor, *F* [-]
		Reynolds Number* [-]	f_z in Eqs. (3) & (4)	$(\Delta P/\Delta L)_{axial}$ [Pa/m]	$(\Delta P/\Delta L)_{Grid}$ [Pa/m]		
113	53.91	97531.53	0.01856	1248.53	140978.99	40807.30	0.2806
100	47.72	86333.74	0.01905	1005.10	110465.18	32072.92	0.2812
90	42.93	77668.44	0.01949	833.01	89403.30	26052.08	0.2821
80	38.16	69038.83	0.02000	676.04	70640.08	20708.33	0.2836
70	33.36	60355.70	0.02061	532.95	53988.45	15906.25	0.2848
60	28.59	51726.72	0.02134	405.88	39654.66	11781.25	0.2869
50	23.8	43062.06	0.02227	293.90	27482.36	8244.80	0.2893
40	19.08	34524.83	0.02346	199.44	17665.56	5375.00	0.2930
30	14.29	25858.26	0.02517	120.37	9909.76	3062.50	0.2969
20	9.55	17284.71	0.02789	59.84	4427.81	1416.67	0.3064
15	7.17	12980.42	0.03010	36.54	2497.13	812.50	0.3107
10	4.77	8639.17	0.03372	18.22	1106.14	369.80	0.3178
7.5	3.59	6504.86	0.03665	11.27	627.11	218.75	0.3309
5	2.38	4315.13	0.04160	5.666	275.96	109.38	0.3758
3	1.43	2596.21	0.03503	1.450	99.90	46.88	0.4547
2	0.95	1727.20	0.03705	0.9929	44.21	15.63	0.3309
1	0.48	839.71	0.07622	0.4827	10.45	6.25	0.5519

* Reynolds numbers are calculated based on the physical velocity in the porous region in the CFD simulations, and so slightly different from the given values in the reference [4] are observed.

Table 5: Verification of the Derived Hydraulic Resistance Correlation by Using CFD Simulations

Power Level [%]	Mass Flow Rate [kg/s]	Simulations			② Measured (iHELP) Averaged $(\Delta P)_{GP's}$ [kPa]	Errors (|①-②|/②) [%]
		Axial Velocity at Axial Mid Position [m/s]	y+ Value at the Centroids of Near-wall Cells [-]	① ΔP over 0.64m at Axial Mid Position [Pa]		
113	53.91	1.531	42.5 ~ 416.0	26161	26.12	0.1692
100	47.72	1.355	37.6 ~ 373.0	20529	20.53	0.0940
90	42.93	1.219	34.0 ~ 340.0	16639	16.67	0.2051
80	38.16	1.084	30.4 ~ 307.0	13173	13.25	0.6076
70	33.36	0.9473	27.0 ~ 273.0	10096	10.16	0.6386
60	28.59	0.8119	24.0 ~ 238.0	7447.0	7.54	1.233
50	23.8	0.6759	21.4 ~ 203.0	5199.4	5.28	1.464
40	19.08	0.5419	19.8 ~ 167.0	3389.8	3.44	1.459
30	14.29	0.4059	19.1 ~ 130.0	1963.1	1.96	0.1582
20	9.55	0.2713	18.2 ~ 91.5	949.03	0.907	4.631
15	7.17	0.2038	17.0 ~ 71.4	583.66	0.520	12.25
10	4.77	0.1356	15.0 ~ 50.2	309.58	0.237	30.62
7.5	3.59	0.1021	13.4 ~ 39.4	209.82	0.14	49.87
5	2.38	0.06773	15.0 ~ 28.4	132.67	0.07	89.53
3	1.43	0.04073	11.8 ~ 28.4	90.972	0.03	> 100
2	0.95	0.02710	10.0 ~ 15.2	77.331	0.01	> 100
1	0.48	0.01211	8.0 ~ 12.0	71.743	0.004	> 100